ISSN 1063-7834, Physics of the Solid State, 2014, Vol. 56, No. 3, pp. 449–455. © Pleiades Publishing, Ltd., 2014.
Original Russian Text © I.A. Sluchinskaya, A.I. Lebedev, A. Erko, 2014, published in Fizika Tverdogo Tela, 2014, Vol. 56, No. 3, pp. 442–447.

DIELECTRICS

Structural Position and Charge State of Nickel in $SrTiO_3$

I. A. Sluchinskaya[a], *, A. I. Lebedev[a], and A. Erko[b]

[a] *Moscow State University, Moscow, 119991 Russia*

* *e-mail: irinasluch@nm.ru*

[b] *Helmholtz-Zentrum, BESSY GmbH, Albert-Einstein-Strasse 15, 12489 Berlin, Germany*

Received August 9, 2013

Abstract—The properties of nickel-doped strontium titanate are studied using X-ray diffraction and XAFS spectroscopy. It is shown that, independently of preparation conditions, the most stable phases in the samples are single-phase $SrTi_{1-x}Ni_xO_3$ solid solution and $NiTiO_3$ which can coexist. According to the EXAFS data, in the single-phase $SrTi_{0.97}Ni_{0.03}O_3$ sample the nickel atoms substitute the titanium atoms and are on-center ones. In this case, no distortions of the oxygen octahedron which would appear in the presence of oxygen vacancies in the nickel environment were detected. An analysis of the XANES spectra shows that the nickel charge state in $NiTiO_3$ is 2+, whereas in the $SrTi_{1-x}Ni_xO_3$ solid solution it is close to 4+. It is shown that the strongest light absorption in doped samples is associated with the presence of tetravalent Ni in the $SrTi_{1-x}Ni_xO_3$ solid solution. This doping seems to be the most promising for solar energy converters based on the bulk photovoltaic effect.

DOI: 10.1134/S1063783414030329

1. INTRODUCTION

The bulk photovoltaic effect consists in the emergence of a photocurrent and very high photovoltages when illuminating homogeneous crystals having no inversion center [1]. The idea of practical applications of this effect in ferroelectrics for solar energy conversion was discussed as early as in the 1970s [2]. However, the quantum yield of this effect is usually small because of the short lifetime of photoexcited carriers, and this idea was regarded as unproductive. Recently, an interest in ferroelectric oxides with the perovskite structure revived again as new ideas how to increase the efficiency of solar energy converters based on the bulk photovoltaic effect have been proposed [3, 4]. The main disadvantage of the ferroelectric oxides is their relatively large bandgap, because of which they absorb only a small fraction of the solar energy. Recent theoretical studies showed that the substitution of Ti atoms at the *B* site of the perovskite structure with a divalent impurity with d^8 electronic configuration (Ni, Pd, Pt), compensated by an oxygen vacancy, decreases the band gap and the resulting perovskites are polar semiconductor oxides [5, 6].

Additional interest to the study of the nickel impurity is associated with the results obtained in recent experimental and theoretical studies of new materials, i.e., recently synthesized $PbNiO_3$ with a very high calculated spontaneous polarization [7–9] and $BiNiO_3$ with unexpected charge states of nickel and bismuth atoms [10].

Furthermore, the search for new magnetic off-center impurities, which can cause simultaneous ferroelectric and magnetic ordering in incipient ferroelectrics and the appearance of magnetoelectric coupling, is still important. Materials with such properties belong to multiferroics. An example of such a material can be $SrTiO_3$ doped with Mn impurity at the *A* site, in which a new type of magnetoelectric coupling was recently discovered [11, 12]. Nickel-doped samples could be an another example.

Since the doping impurity can enter several different sites of the perovskite structure and stay in them in different charge states, the aim of this work was to study the structural position and charge state of the Ni impurity in $SrTiO_3$ prepared under different conditions using XAFS spectroscopy. We planned to check the possibility of obtaining samples with divalent Ni at the *B* site, the possibility of incorporating the Ni impurity into the *A* site, and to determine the correlation between optical properties of samples, on the one hand, and the structural position and charge state of the impurity, on the other hand. The choice of $SrTiO_3$ was dictated by the fact that we have previously determined the structural positions and charge states of a number of 3*d* impurities (Mn [13, 14], Co [15], Fe [16]) in this material; their comparative analysis can make it possible to find new promising impurities for solar energy converters.

2. SAMPLES AND EXPERIMENTAL TECHNIQUE

Nickel-doped $SrTiO_3$ samples with the impurity concentration of 2–3% and various deviation from

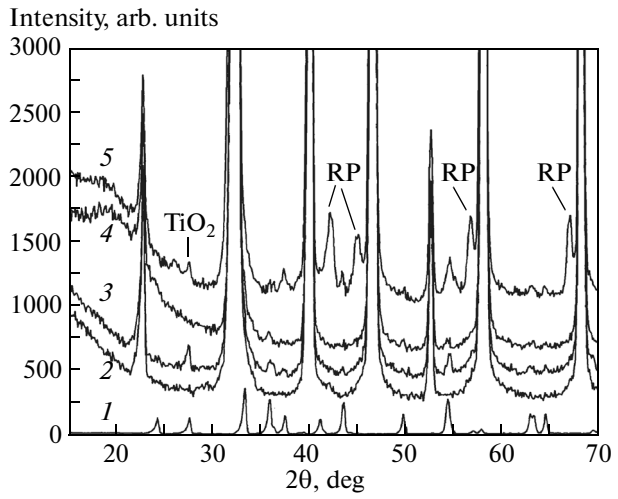

Fig. 1. X-ray diffraction patterns of (*1*) $NiTiO_3$, (*2*) $SrTi_{0.97}Ni_{0.03}O_3$ annealed at 1500°C, (*3*) $Sr_{0.98}Ni_{0.02}TiO_3$ annealed at 1100°C, (*4*) $Sr_{0.98}Ni_{0.02}TiO_3$ annealed at 1500°C, and (*5*) $SrTi_{0.97}Ni_{0.03}O_3$ annealed at 1100°C. Arrows indicate the reflections of TiO_2 and Ruddlesden–Popper (RP) phases.

stoichiometry were prepared by the solid-state reaction method. The starting components were $SrCO_3$, nanocrystalline TiO_2 prepared by the hydrolysis of tetrapropyl orthotitanate and dried at 500°C, and $Ni(CH_3COO)_2 \cdot 4H_2O$. The components were weighed in required proportions, ground in acetone, and annealed in air in alumina crucibles at 1100°C for 8 h. The obtained powders were ground again and repeatedly annealed under the same conditions. Some samples were additionally annealed in air at 1500°C for 2 h. To incorporate nickel into the *A* and *B* sites of the perovskite structure, the composition of the samples was intentionally deviated from the stoichiometry toward excess of titanium or strontium.

The reference samples NiO, $NiTiO_3$, and $BaNiO_{3-\delta}$ used to determine the Ni impurity charge state in $SrTiO_3$ were prepared as follows. The NiO sample was obtained by thermal decomposition of $Ni(CH_3COO)_2 \cdot 4H_2O$. Two other samples were prepared by the solid-state reaction method in air: the $NiTiO_3$ sample was obtained from $Ni(CH_3COO)_2 \cdot 4H_2O$ and TiO_2 at 1100°C, the $BaNiO_{3-\delta}$ sample was prepared from BaO_2 and NiO at 650°C. The phase composition of the obtained samples was checked by the X-ray diffraction.

The spectra of the extended X-ray absorption fine structure (EXAFS) and X-ray absorption near-edge structure (XANES) were measured at KMC-2 station of the BESSY synchrotron radiation source (the beam energy is 1.7 GeV, the maximum beam current is 290 mA) at the Ni *K*-edge (8.34 keV) at 300 K. The radiation was monochromatized by a $Si_{1-x}Ge_x(111)$ double-crystal monochromator. The EXAFS spectra were measured in fluorescence mode. The radiation intensity incident on the sample (I_0) was measured using an ionization chamber, the X-ray fluorescence intensity (I_f) was measured by a silicon energy dispersive RÖNTEC X-flash detector with an active area of 10 mm^2.

The EXAFS oscillating function $\chi(k)$ was extracted from the fluorescence excitation spectra $\mu(E) = I_f/I_0$ (here E is the X-ray photon energy) by the conventional method [17, 18]. After subtracting the pre-edge background, the monotonic atomic part of the spectrum $\mu_0(E)$ was extracted using splines, and the dependence of $\chi = (\mu - \mu_0)/\mu_0$ was calculated as a function of photoelectron wave vector $k = (2m(E - E_0)/\hbar^2)^{1/2}$. The energy corresponding to the inflection point at the absorption edge was taken as the energy origin E_0. For each sample three spectra were recorded, they were then independently processed, and then the obtained curves $\chi(k)$ were averaged.

Information about the first three shells was isolated from the obtained curves $\chi(k)$ using the direct and inverse Fourier transforms with a modified Hanning window. The distances R_j and Debye–Waller factors σ_j^2 for the *j*th shell ($j = 1-3$) were determined by minimizing the root-mean-square deviation between experimental and calculated $k^2\chi(k)$ curves. In addition to the parameters R_j and σ_j^2, the energy origin correction dE_0 was simultaneously varied. The coordination numbers were considered fixed at the values given by a structural model. The number of adjustable parameters (8) was approximately a half of the number of independent data points, $N_{ind} = 2\Delta k\Delta R/\pi \approx 16$.

The scattering amplitudes and phase shifts, the phase shift of the central atom, and the photoelectron mean free path as a function of k, required to calculate the theoretical curves $\chi(k)$, were computed using the FEFF6 software [19].

The EXAFS spectra were also processed with the widely used IFEFFIT software package [20]. The experimental EXAFS function was extracted using the ATHENA program; its fitting to the theoretical curve calculated for a given structural model was performed using the ARTEMIS program. In this approach, the amplitudes and phases shifts for all single- and multiple-scattering paths were also calculated using the FEFF6 software. The results obtained with two different processing methods were in good agreement.

3. RESULTS

3.1. X-Ray Data

The diffraction patterns of all studied samples are shown in Fig. 1. It is seen that the $SrTi_{0.97}Ni_{0.03}O_3$ sample annealed at 1500°C is the only single-phase sam-

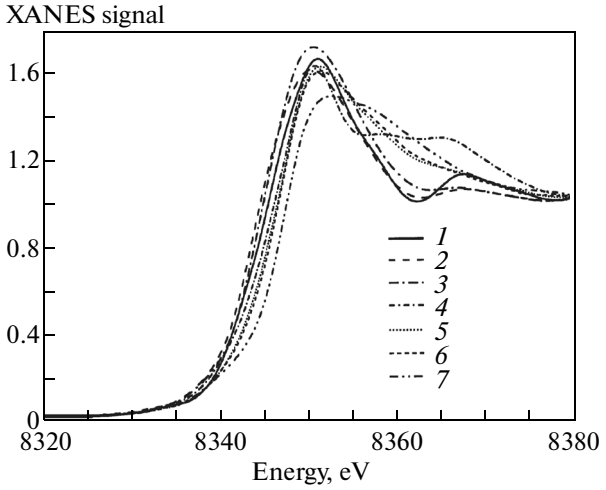

Fig. 2. XANES spectra for $SrTiO_3$(Ni) samples and reference compounds of nickel: (*1*) NiO, (*2*) $NiTiO_3$, (*3*) $Sr_{0.98}Ni_{0.02}TiO_3$ annealed at 1500°C, (*4*) $BaNiO_{3-\delta}$, (*5*) $SrTi_{0.97}Ni_{0.03}O_3$ annealed at 1100°C, (*6*) $Sr_{0.98}Ni_{0.02}TiO_3$ annealed at 1100°C, and (*7*) $SrTi_{0.97}Ni_{0.03}O_3$ annealed at 1500°C.

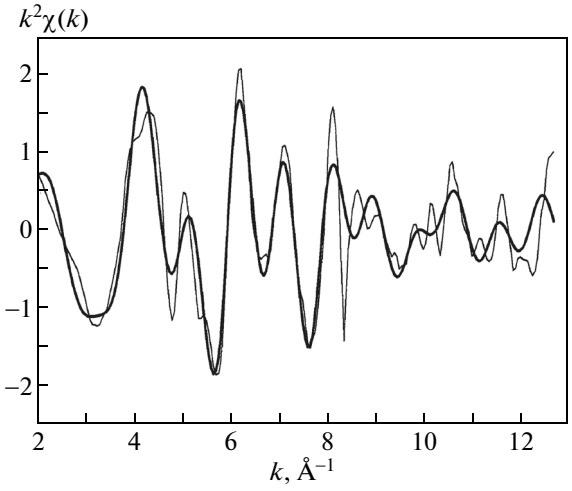

Fig. 3. EXAFS spectrum obtained at the Ni *K*-edge at 300 K for the $SrTi_{0.97}Ni_{0.03}O_3$ sample annealed at 1500°C (thin line) and its best theoretical fit (thick line).

ple with the cubic perovskite structure; the diffraction patterns of other samples exhibit additional reflections. For the $SrTi_{0.97}Ni_{0.03}O_3$ and $Sr_{0.98}Ni_{0.02}TiO_3$ samples annealed at 1100°C, along with the reflections characteristic of the perovskite phase, additional reflections were observed, which indicate the presence of a small amount of TiO_2 and, presumably, $NiTiO_3$ in these samples. The identification of the possible NiO phase was complicated by the closeness of the position of its reflections to the position of $NiTiO_3$ reflections. In addition, stronger lines of the $Sr_3Ti_2O_7$ and $Sr_4Ti_3O_{10}$ Ruddlesden–Popper phases were observed in the $SrTi_{0.97}Ni_{0.03}O_3$ sample annealed at 1100°C. In the $Sr_{0.98}Ni_{0.02}TiO_3$ sample annealed at 1500°C, only one additional $NiTiO_3$ phase was detected.

Since barium nickelate $BaNiO_{3-\delta}$ is a defect phase with the parameter δ depending on preparation conditions, the actual composition of our $BaNiO_{3-\delta}$ sample was determined using the dependence of the hexagonal lattice parameters of this phase on δ [21]. In our sample, the hexagonal lattice parameters were a = 5.568(1) Å and c = 4.838(1) Å, which correspond to $\delta \approx 0.4$.

3.2. Analysis of XANES Spectra

To determine the charge state of the Ni impurity in $SrTiO_3$, the absorption edge position in the XANES spectra of the samples under study was compared with the edge positions in the reference compounds. The XANES spectra of all studied samples and three reference compounds are shown in Fig. 2.

A comparison of the spectra of the $Sr_{0.98}Ni_{0.02}TiO_3$ sample annealed at 1500°C with the spectra of cubic NiO and rhombohedral $NiTiO_3$ (with the ilmenite structure) shows that their absorption edges are very close. It can be concluded that the Ni impurity in this sample is in the 2+ charge state. The absorption edges for the $SrTi_{0.97}Ni_{0.03}O_3$ and $Sr_{0.98}Ni_{0.02}TiO_3$ samples annealed at 1100°C almost coincide and are close to the absorption edge in the $BaNiO_{3-\delta}$ reference compound. In the single-phase $SrTi_{0.97}Ni_{0.03}O_3$ sample annealed at 1500°C, the absorption edge is shifted to higher energies (by 2.5, 2.9, and 1.3 eV in comparison with NiO, $NiTiO_3$, and $BaNiO_{3-\delta}$, respectively).

3.3. Analysis of EXAFS Spectra

The structural position of the Ni impurity was determined from the analysis of the EXAFS spectra. The typical EXAFS spectrum $k^2\chi(k)$ for the single-phase $SrTi_{0.97}Ni_{0.03}O_3$ sample annealed at 1500°C and its best theoretical fit which takes into account the multiple-scattering effects are shown in Fig. 3. The best agreement between the calculated and experimental spectra is achieved in the model in which Ni atoms substitute Ti atoms in $SrTiO_3$. The interatomic distances and Debye–Waller factors for three nearest shells in this sample are given in the table. The small Debye–Waller factors for the first and second shells, which are typical for the thermal vibrations in perovskites at 300 K, allow to draw the following conclusions: (i) they exclude the possibility of off-centering of Ni atoms and (ii) they indicate the absence of the oxygen vacancies near the impurity atoms.

An analysis of the EXAFS spectra allowed us to accurately determine the composition of the second phase precipitating in the $SrTi_{0.98}Ni_{0.02}O_3$ sample

Structural parameters obtained from the EXAFS data analysis for the $SrTi_{0.97}Ni_{0.03}O_3$ sample annealed at 1500°C (R_i is the distance to the ith shell, σ_i^2 is the Debye–Waller factor for this shell)

Shell	R_i, Å	σ_i^2, Å^2	Atom
1	1.914(4)	0.0035(6)	O
2	3.342(6)	0.0084(7)	Sr
3	3.877(4)	0.0053(5)	Ti

annealed at 1500°C. Although the distances to the nearest atoms and the coordination numbers for the first shell of nickel in NiO and $NiTiO_3$ are close, the coordination numbers for the second shell in these compounds differ by a factor of 3. A comparison of the Fourier-transforms of the EXAFS spectra for the sample under consideration and $NiTiO_3$ and NiO reference compounds shows a better agreement of its spectrum with the spectrum of $NiTiO_3$ (Fig. 4). This means that among two possible phases, $NiTiO_3$ and NiO, the $NiTiO_3$ phase is precipitated in our sample.

As for the $SrTi_{0.97}Ni_{0.03}O_3$ and $Sr_{0.98}Ni_{0.02}TiO_3$ two-phase samples annealed at 1100°C, the comparison of their EXAFS spectra with that of the single-phase solid solution and that of $NiTiO_3$ shows that the spectra of the samples under consideration can be regarded as a superposition of the spectra of $NiTiO_3$ and of the solid solution in a ratio close to 1:1.

The optical properties of the samples under study agree with the data obtained above. The $Sr_{0.98}Ni_{0.02}TiO_3$ sample annealed at 1500°C was pale brown; the $SrTi_{0.97}Ni_{0.03}O_3$ and $Sr_{0.98}Ni_{0.02}TiO_3$ samples annealed at 1100°C were dark brown; the single-phase $SrTi_{0.97}Ni_{0.03}O_3$ sample annealed at 1500°C was almost black, and the $NiTiO_3$ sample was bright yellow. Thus, the sample color is determined by the relative amount of black $SrTi_{1-x}Ni_xO_3$ and yellow $NiTiO_3$.

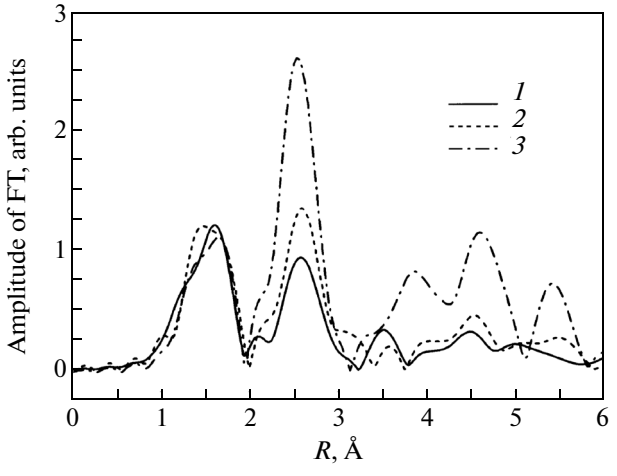

Fig. 4. Comparison of the Fourier transforms of the EXAFS $k^2\chi(k)$ spectra obtained for (*1*) $Sr_{0.98}Ni_{0.02}TiO_3$ sample annealed at 1500°C and reference (*2*) $NiTiO_3$ and (*3*) NiO compounds.

4. DISCUSSION

A combined analysis of X-ray and EXAFS data shows that the $SrTi_{0.97}Ni_{0.03}O_3$ sample annealed at 1500°C is a single-phase solid solution in which the Ni atoms substitute the Ti atoms at the *B* sites and are on-center. This means that the nickel solubility at the *B* sites in $SrTiO_3$ exceeds 3% at 1500°C. In the sample with a nominal composition of $SrTi_{0.97}Ni_{0.03}O_3$ annealed at 1100°C, the appearance of the reflections of $NiTiO_3$ and of the Ruddlesden–Popper phases indicates that some of the Ni atoms are involved in the $NiTiO_3$ formation, while the others remain at the *B* sites. In this case, the "untapped" Sr atoms form the SrO planes which are embedded into the perovskite structure to form $Sr_3Ti_2O_7$ and $Sr_4Ti_3O_{10}$ phases.

In attempting to incorporate Ni atoms into the *A* sites of strontium titanate upon annealing at 1500°C (the samples with a nominal composition of $Sr_{0.98}Ni_{0.02}TiO_3$), the $NiTiO_3$ second phase is precipitated. In this case, the nickel concentration in the solid solution phase is low as it follows from the EXAFS data and the sample color. On the contrary, upon annealing of the $Sr_{0.98}Ni_{0.02}TiO_3$ sample at a lower temperature (1100°C), the nickel in the sample is in a mixture of $NiTiO_3$ and $SrTi_{1-x}Ni_xO_3$ solid solution as it follows from the XANES, EXAFS data, and the sample color. The incorporation of Ni into $SrTiO_3$ is confirmed by precipitation of a small amount of the TiO_2 phase (its appearance is a consequence of the removing of a part of Ti from the *B* sites when doping strontium titanate with nickel).

As for the appearance of the TiO_2 phase in the $SrTi_{0.97}Ni_{0.03}O_3$ sample upon its annealing at 1100°C, we suppose that the appearance of this phase is possible for kinetic reasons. The solid solution is apparently formed as a result of a chain of chemical reactions in which the nickel titanate phase is formed first and its subsequent dissolving during the reaction with SrO is complicated. As a result, a mixture of the solid solution, nickel titanate, and TiO_2 is formed in the samples annealed at 1100°C. At a higher annealing temperature, the kinetic processes are faster, the reaction is completed, and the sample composition is fully controlled by the deviation from stoichiometry.

Thus, the stable phases in the studied samples are the single-phase $SrTi_{1-x}Ni_xO_3$ solid solution and $NiTiO_3$; their ratio depends on the deviation from stoichiometry and the annealing temperature. It is impossible to incorporate nickel into the *A* site of strontium titanate. The low stability of Ni at the *A* site

of strontium titanate is probably a consequence of the significant difference of the Ni^{2+} and Sr^{2+} ionic radii (the twelvefold configuration is not typical of nickel; at a coordination number of 6, the Ni^{2+} ionic radius (0.69 Å) is much smaller than the Sr^{2+} ionic radius (1.18 Å) [22]).

The XANES data used to determine the nickel charge state are in complete agreement with X-ray and EXAFS data. In the sample with a nominal composition of $Sr_{0.98}Ni_{0.02}TiO_3$ annealed at 1500°C, in which nickel is in the $NiTiO_3$ phase, the Ni charge state is identical to its charge state in NiO and $NiTiO_3$ and is 2+. In the single-phase $SrTi_{0.97}Ni_{0.03}O_3$ sample annealed at 1500°C, the absorption edge shift with respect to $NiTiO_3$ is maximum and is about twice the shift between $NiTiO_3$ and $BaNiO_{3-\delta}$ reference compounds. If, following [21], we proceed from the number of ions, their nominal charges, and the value $\delta \approx 0.4$ determined from the lattice parameters, the average nickel charge in $BaNiO_{3-\delta}$ is $(4 - 2\delta) = 3.2$. Then, according to the shift of the absorption edge in the $SrTi_{0.97}Ni_{0.03}O_3$ sample annealed at 1500°C, the nickel charge state in this sample should be close to 4+. For the $SrTi_{0.97}Ni_{0.03}O_3$ and $Sr_{0.98}Ni_{0.02}TiO_3$ samples annealed at 1100°C, which we consider as a mixture of two nickel-containing phases in the ratio close to 1 : 1, the edge position is intermediate between the edge positions in two stable phases and is close to the edge position in $BaNiO_{3-\delta}$ (~3+).

It should be noted that the problem of the Ni charge state in $SrTi_{0.97}Ni_{0.03}O_3$ is not so simple. The Ni charge state in $BaNiO_{3-\delta}$ is still discussed; in particular, the doubts were expressed [23] on the adequacy of its formal determination based on the number of ions and their nominal charges. In [23], the Mössbauer spectroscopy data for $BaNiO_3$ indicate the Ni charge state close to 4+, whereas the photoelectron spectroscopy data give the value close to 3+. The authors of [23] proposed a model in which Ni is trivalent, and its charge is compensated by a hole bound by one or two negatively charged oxygen ions. If this is the case, the Ni charge state determined from the absorption edge shift in the $SrTi_{0.97}Ni_{0.03}O_3$ solid solution should be closer to 3+. However, this explanation contradicts the fact that no distortion of the oxygen octahedron was observed in our EXAFS spectra, whereas the hole localization at one or two oxygen ions should cause its distortion.

At the same time, the experimental studies of XANES spectra of the Li_xNiO_2 compound used in lithium batteries showed that a change in the degree of intercalation x changes the Ni charge state from 2+ to 4+ and shifts the absorption edge in the XANES spectra by ~3.5 eV [24]. This shift is consistent with the shift of 2.9 eV we observed between $NiTiO_3$ and the $SrTi_{0.97}Ni_{0.03}O_3$ sample annealed at 1500°C. Furthermore, the Ni–O interatomic distance (1.914 Å) we determined from the EXAFS measurements appears smaller than the sum of the Ni^{3+} and O^{2-} ionic radii (0.56 + 1.4 = 1.96 Å) and is closer to the sum of the Ni^{4+} and O^{2-} ionic radii (0.48 + 1.4 = 1.88 Å). One more argument in favor of tetravalent nickel can be the small Debye–Waller factors σ_1^2 indicating the absence of the Ni displacements from the B sites in the $SrTi_{0.97}Ni_{0.03}O_3$ solid solution. If the nickel atoms were incorporated into the crystal in the Ni^{3+} charge state, this would require its charge compensation by an oxygen vacancy located nearby the impurity atom (such axial Ni^{3+}–V_O centers with the Ni displacement up to ~0.3 Å from the octahedron center were observed in the electron paramagnetic resonance (EPR) spectra in [25, 26]). However, our EXAFS measurements detected no noticeable distortions of oxygen octahedra surrounding the nickel atoms, and the Ni coordination number for the first shell remains close to 6.

Therefore, we come to the conclusion that the nickel charge state at the B site of strontium titanate is close to 4+; this conclusion is not consistent with the assumption made previously [5, 6] that in the related ferroelectric $PbTiO_3$ nickel is in the 2+ charge state. Although the question about the actual Ni charge state in this material is to be studied experimentally, the obtained data indicate that the strong light absorption in nickel-doped $SrTiO_3$ should be associated with the tetravalent nickel.

From the viewpoint of possible applications of doped perovskites in solar energy conversion, it is of interest to compare the properties of strontium titanate doped with nickel and with other 3d elements [13–16]. The absorption spectra of these samples are systematically shifted to the infrared region as the atomic number of the element increases from Mn to Ni: manganese-doped samples are greenish-brown; iron, cobalt, and nickel impart brown, dark brown, and almost black color, respectively, to the samples. Thus, to create samples that strongly absorb light in the entire visible region, the nickel doping seems to be the most promising.

It is interesting that the small value of the Debye–Waller factor for the first shell ($\sigma_1^2 \approx 0.0035$ Å^2) excludes the possibility of Jahn–Teller instability of the Ni^{4+} ion, which is possible for the d^6 octahedral configuration. Indeed, the Jahn–Teller instability of Ni^{4+} in Li_xNiO_2 manifests itself as the oxygen octahedron distortions with the Ni–O bond lengths of 1.88 and 2.08 Å. In the EXAFS spectra of this compound, the oxygen atoms should look like one shell with an average interatomic distance of 1.947 Å and a static Debye–Waller factor of 0.009 Å^2. The latter value is much more than our experimental value of σ_1^2.

The interpretation of our data on the nickel charge state in strontium titanate differs much from the con-

clusions of earlier studies. A comparison with the data of [27] in which $SrTiO_3$(Ni) samples were also studied by the XAFS spectroscopy shows that the XANES and EXAFS spectra obtained in our work and in [27] are qualitatively different. For example, the absorption edge shift in $SrTiO_3$(Ni) with respect to NiO was only 1.1 eV in [27], whereas it was 2.5 eV in this work. In addition, even the sample color is different (beige in [27] and almost black in the present work). We believe that these differences in the sample properties result from the different methods of their preparation (solid-state reaction method in our case and hydrothermal synthesis at 150°C in [27]). In [25, 26], single crystals of $SrTiO_3$(Ni) were studied by the EPR method. In these studies, the EPR spectra related to Ni^{3+}–V_O axial complexes and the spectra attributed to Ni^{2+} and Ni^{3+} "cubic" centers were systematically observed [25]. Unfortunately, no arguments on the basis which the conclusion about the charge states of the Ni impurity were made were presented in [25], and a possible interpretation of the EPR spectra as those of Ni^{4+} was not discussed.

5. CONCLUSIONS

The study of nickel-doped strontium titanate using X-ray diffraction and XAFS spectroscopy allowed us to draw the following conclusions.

(i) The preparation conditions of single-phase nickel-doped $SrTiO_3$ samples with the impurity concentration up to 3% were found. In attempting to incorporate the impurity into the *A* site, the $NiTiO_3$ second phase is precipitated. Independently of the preparation conditions, the most stable phases in the samples are the single-phase $SrTi_{1-x}Ni_xO_3$ solid solution and $NiTiO_3$ phase which can coexist.

(ii) According to the EXAFS data, in the single-phase $SrTi_{0.97}Ni_{0.03}O_3$ sample, the Ni atoms substitute the Ti atoms and are on-center. No distortions of oxygen octahedra which could appear as a result of the presence of the oxygen vacancies in the Ni environment were detected.

(iii) An analysis of the XANES spectra showed that the nickel charge state in $NiTiO_3$ is 2+; in the $SrTi_{1-x}Ni_xO_3$ solid solution it is close to 4+.

(iv) It was shown that the strongest light absorption in doped samples is associated with the presence of tetravalent nickel in the $SrTi_{1-x}Ni_xO_3$ solid solution. This doping seems to be the most promising for developing of solar energy converters that exploit the bulk photovoltaic effect.

In the future, we plan to perform similar experiments on ferroelectric $BaTiO_3$ doped with 3*d* elements to test the possibility of obtaining the polar materials with similar optical and physical properties, in which the bulk photovoltaic effect could be observed for photons in the entire spectrum of solar radiation.

ACKNOWLEDGMENTS

I.A.S. and A.I.L. acknowledge the Russian–German laboratory for financial support and hospitality during their stay at BESSY.

This work was supported by the Russian Foundation for Basic Research (project no. 13-02-00724).

REFERENCES

1. B. I. Sturman and V. M. Fridkin, *The Photovoltaic and Photorefractive Effects in Noncentrosymmetric Materials* (Nauka, Moscow, 1992; CRC Press, Boca Raton, Florida, United States, 1992).
2. A. M. Glass, D. von der Linde, and T. J. Negran, Appl. Phys. Lett. **25**, 233 (1974).
3. M. Qin, K. Yao, and Y. C. Liang, Appl. Phys. Lett. **93**, 122904 (2008).
4. M. Alexe and D. Hesse, Nat. Commun. **2**, 256 (2011).
5. J. W. Bennett, I. Grinberg, and A. M. Rappe, J. Am. Chem. Soc. **130**, 17409 (2008).
6. G. Y. Gou, J. W. Bennett, H. Takenaka, and A. M. Rappe, Phys. Rev. B: Condens. Matter **83**, 205115 (2011).
7. Y. Inaguma, M. Yoshida, T. Tsuchiya, A. Aimi, K. Tanaka, T. Katsumata, and D. Mori, J. Phys.: Conf. Ser. **215**, 012131 (2010).
8. Y. Inaguma, K. Tanaka, T. Tsuchiya, D. Mori, T. Katsumata, T. Ohba, K.-i. Hiraki, T. Takahashi, and H. Saitoh, J. Am. Chem. Soc. **133**, 16920 (2011).
9. X. F. Hao, A. Stroppa, S. Picozzi, A. Filippetti, and C. Franchini, Phys. Rev. B: Condens. Matter **86**, 014116 (2012).
10. M. Azuma, S. Carlsson, J. Rodgers, M. G. Tucker, M. Tsujimoto, S. Ishiwata, S. Isoda, Y. Shimakawa, M. Takano, and J. P. Attfield, J. Am. Chem. Soc. **129**, 14433 (2007).
11. V. V. Shvartsman, S. Bedanta, P. Borisov, W. Kleemann, A. Tkach, and P. M. Vilarinho, Phys. Rev. Lett. **101**, 165704 (2008).
12. W. Kleemann, S. Bedanta, P. Borisov, V. V. Shvartsman, S. Miga, J. Dec, A. Tkach, and P. M. Vilarinho, Eur. Phys. J. B **71**, 407 (2009).
13. A. I. Lebedev, I. A. Sluchinskaya, A. Erko, and V. F. Kozlovskii, JETP Lett., **89** (9), 457 (2009).
14. I. A. Sluchinskaya, A. I. Lebedev, and A. Erko, Bull. Russ. Acad. Sci.: Phys. **74** (9), 1235 (2010).
15. I. A. Sluchinskaya, A. I. Lebedev, and A. Erko, in *Abstracts of Papers of the XIX All-Russian Conference on Physics of Ferroelectrics (VKS-19), Moscow, June 20–23, 2011*, p. 116.
16. I. A. Sluchinskaya, A. I. Lebedev, V. F. Kozlovskii, and A. Erko, in *Abstracts of Papers of the VIII National Conference "X-Rays, Synchrotron Radiation, Neutrons and Electrons for Nanosystems and Materials Research: Nano-Bio-Info-Cognitive Technologies," Moscow, November 14–18, 2011*, p. 347.
17. A. I. Lebedev, I. A. Sluchinskaya, V. N. Demin, and I. Manro, Izv. Akad. Nauk SSSR, Ser. Fiz. **60** (10), 46 (1996).

18. A. I. Lebedev, I. A. Sluchinskaya, V. N. Demin, and I. H. Munro, Phys. Rev. B: Condens. Matter **55**, 14770 (1997).
19. FEFF project home page, http://leonardo.phys.washington.edu/feff/.
20. IFEFFIT project home page, http://cars9.uchicago.edu/ifeffit/.
21. M. Arjomand and D. J. Machin, J. Chem. Soc., Dalton Trans. 1055 (1975).
22. R. D. Shannon, Acta Crystallogr., Sect. A: Cryst. Phys., Diffr., Theor. Gen. Crystallogr. **32**, 751 (1976).
23. R. Gottschall, R. Schöllhorn, M. Muhler, N. Jansen, D. Walcher, and P. Gütlich, Inorg. Chem. **37**, 1513 (1998).
24. A. N. Mansour and C. A. Melendres, J. Phys. Chem. A **102**, 65 (1998).
25. K. A. Müller, W. Berlinger, and R. S. Rubins, Phys. Rev. **186**, 361 (1969).
26. S.-Y. Wu, J.-Z. Lin, Q. Fu, and H.-M. Zhang, Phys. Scr. **75**, 147 (2007).
27. A. M. Beale, M. Paul, G. Sankar, R. J. Oldman, C. R. A. Catlow, S. French, and M. Fowles, J. Mater. Chem. **19**, 4391 (2009).

Translated by A. Kazantsev